Thermochimica Acta 495 (2009) 101–107

Contents lists available at ScienceDirect

Thermochimica Acta

journal homepage: www.elsevier.com/locate/tca

# Non-steady effective thermal properties of semi-infinite unidirectional fiber-reinforced composites using thermal wave method

Xue-Qian Fang[a,*], Xiao-Hua Wang[b], Dao-Bin Wang[a], Chao Hu[c]

[a] Department of Engineering Mechanics, Shijiazhuang Railway Institute, Bei Erhuan Road, Shijiazhuang, Hebei 050043, China
[b] Department of Computer and Information Engineering, Shijiazhuang Railway Institute, Shijiazhuang 050043, China
[c] School of Aerospace Engineering & Applied Mechanics, Tongji University, Shanghai 200092, China

ARTICLE INFO

*Article history:*
Received 19 February 2009
Received in revised form 31 May 2009
Accepted 8 June 2009
Available online 18 June 2009

*Keywords:*
Semi-infinite fiber-reinforced composites
Effective medium method
Non-steady effective thermal properties
Image method

ABSTRACT

Photothermal techniques and effective medium method combining with image method are applied to investigate the non-steady effective thermal properties of semi-infinite unidirectional fiber-reinforced composites, and the effect of the semi-infinite surface on the non-steady effective thermal properties is considered. The dispersion relation for the effective wave number in the semi-infinite random composites is derived. The image method is used to satisfy the adiabatic boundary condition at the semi-infinite surface. The numerical solutions of the non-steady effective thermal properties are obtained by using an iterative scheme. Analyses show that the variation of the non-steady effective thermal properties near the semi-infinite surface is significantly different from those of the infinite composite structure. The effects of the circular frequency of thermal waves, the volume fraction of fibers, and the properties contrast ratio on the maximum non-steady effective properties near the surface are examined. Comparison with the steady case is also given.



## 1. Introduction

Composite materials are extensively used in engineering fields for thermal transfer applications. The effective thermal conductivity of composites is an important property applied in electronic packing, thermal insulation, heat spreader, etc. [1]. To design and manufacture an optimal material system, the development of micromechanics models to accurately predict the effective thermal conductivity of multiphase composite materials is desirable.

Extensive theoretical and experimental studies on the effective thermal conductivity of a two-phase composite material under different loadings have received great interest in recent years. The methods used to measure the thermal conductivity are divided into two groups: the steady-state and the non-steady-state methods. In the first one, the sample is subjected to a constant heat flow. In the second group, a periodic or transient heat flow is established in the sample [2–5]. In the past, much attention has been focused on the problems of steady state.

The earliest models for the thermal behavior of composites assumed that the two components are both homogeneous, and are perfectly bounded across a sharp and distinct interface. The Maxwell solution [6] is the starting point of finding the effective thermal conductivity of two-phase material systems, but it is only valid for very low concentrations of the dispersed phase. Subsequently, many structural models, e.g., parallel, Maxwell–Eucken [7], and effective medium theory models [8], were proposed. Recently, Samantray et al. [9] applied the unit-cell approach to study the effective thermal conductivity of two-phase materials. Based on the effective medium theory, Bagchi and Nomura [10] developed a theoretical model to predict the effective thermal conductivity of an aligned multi-walled nano-tube polymer composite. Based on an equivalent inclusion concept, Hasselman and Johnson [11] extended Maxwell's theory to the systems of spherical inclusion with a contact resistance. The idea of the generalized self-consistent model was also developed by Hashin [12] to determine the effective thermal conductivity of two-phase materials.

In many high-temperature situations, non-steady heat flux is more common. Due to the complexity of non-steady loading, up to the present time, very little work treating the non-steady effective thermal properties has been done. Photothermal techniques have become powerful tools for the thermophysical characterization and non-destructive evaluation (NDE) of various materials in the past few decades. Recently, Monde and Mitsutake [3] proposed a method for determining the thermal diffusivity of solids using an analytical inverse solution for unsteady heat conduction. By using modulated photothermal techniques, Salazar et al. [2] studied the effective thermal diffusivity of composites made of a matrix filled with aligned circular cylinders of a different material. Most recently, Fang and Hu investigated the distribution of dynamic effective thermal properties along the gradation direction of functionally graded

* Corresponding author. Tel.: +86 311 87936542.
*E-mail address:* fangxueqian@163.com (X.-Q. Fang).

0040-6031/$ – see front matter © 2009 Elsevier B.V. All rights reserved.
doi:10.1016/j.tca.2009.06.011

materials by using the Fourier heat conduction law [4] and the non-Fourier heat conduction law [5].

It is well known that in non-destructive evaluation, the periodic or transient heat flow is often established at the surface of a sample, so the model of the semi-infinite structure is more practical. However, because of the effects of the boundaries of the investigated areas, the complex problems such as multiple scattering of thermal waves resulting from the semi-infinite surface may arise. In the past, very few investigations on the thermodynamics of semi-infinite composites have been engaged in. Recently, Terrón et al. have studied the multiple scattering of a plane thermal wave between a subsurface cylinder and the material surface theoretically and experimentally [13]. The multiple scatterings of thermal waves between two cylinders and the semi-infinite surface [14], between a sphere and the semi-infinite surface [15] were also studied by Terrón and his coworkers. The image method has proven to be an efficient way used to satisfy the adiabatic boundary condition. It has been applied to analyze the multiple scattering of thermal waves [13–15], flexural waves [16] and shear waves [17] resulting from semi-infinite surfaces.

Effective medium method (EMM) is a more accurate method for evaluating the effective field and computing the effective properties of composites with randomly distributed inclusions, and has been successfully used in analyzing the wave field in composite materials [18]. By making use of this method, an original inhomogeneous media can be replaced by a homogeneous one with the effective thermodynamic parameters of the former (the homogenization problem). This substitution essentially simplifies the analysis of the propagation of various types of waves in composite materials (non-monochromatic waves, non-plane waves). The effective media that is equivalent to the original composite material is a media with space and time dispersion, and hence, its parameters are functions of frequency of the original field. Through analyzing the non-steady effective parameters, one can obtain the non-steady behavior of composites under high-frequency thermal impact.

The main objective of this paper is to investigate the non-steady effective thermal properties of semi-infinite random unidirectional fiber-reinforced composites by using photothermal techniques. The adiabatic boundary condition at the semi-infinite surface is considered. The effective medium method is applied to analyze the interaction of thermal waves between the randomly distributed fibers in the matrix. The dispersion relation for the effective wave number in the random media is obtained. In the one-fiber problem, the image method is employed to satisfy the adiabatic boundary condition at the semi-infinite surface. Through the numerical examples, the effects of the phase properties, the volume fraction of fibers and the incident wave number on the non-steady effective thermal properties are analyzed.

## 2. Formulation of the thermodynamic problem

Consider a semi-infinite random unidirectional fiber-reinforced composite material, as depicted in Fig. 1. The two-dimensional composite material is common in many previous works [19,20]. The composite material contains a large number $N$ of fibers embedded in the semi-infinite matrix. The long, parallel fibers with identical properties are randomly distributed in the matrix. For simplicity, the discrete fibers are assumed to be fully bonded to the matrix. Let $\lambda_0$, $c_0$, $\rho_0$ be the thermal conductivity, specific heat capacity and mass density of the matrix, and $\lambda$, $c$, $\rho$ those of the fibers. The volume fraction of fibers is denoted by $V_f$.

The global coordinate system of the semi-infinite composite material is denoted by *OXY*. The sample surface is heated by an extended light beam modulated at a frequency $\omega$. The extended light beam can generate a plane thermal wave that propagates along

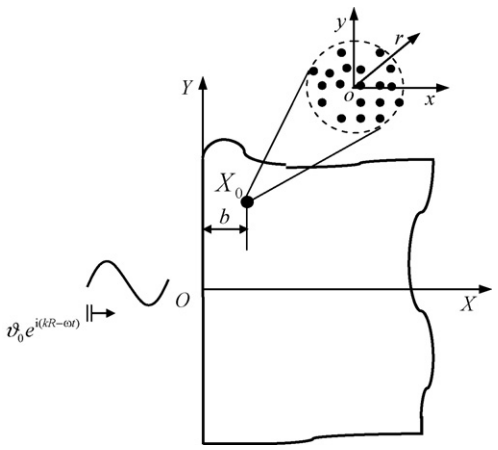


**Fig. 1.** The incidence of extended light beam and representative volume element in a semi-infinite random fiber-reinforced composite material.

the $X$ direction in the material. When the thermal wave propagates in the semi-infinite composite material, the interaction of thermal waves between the randomly distributed fibers and the multiple scattering resulting from the boundary of the structures give rise to the dispersion relations for thermal waves. The propagating wave number of thermal waves varies because of the dispersion relations, and it is denoted as the effective wave number $k_e$.

To analyze the interaction of thermal waves between the randomly distributed fibers, a microscopic representative volume element (RVE) is proposed to represent the microstructure in the neighborhood of a material point in the semi-infinite composite material. For any macroscopic material point $X_0$ near the semi-infinite surface, the corresponding microstructural RVE contains a number of identical fibers embedded in a continuous matrix, so that the overall volume fraction of fibers should be consistent with the macroscopic counterparts $V_f$. As seen in Fig. 1, the whole RVE domain is denoted by $D$, and the microscopic coordinate system *OXY* is constructed with its origin at the material point $X_0$. In the RVE, the effective medium method is employed to derive the non-steady effective thermal properties and wave fields. The image method is also combined with effective medium method to consider the boundary effect of the semi-infinite composite.

## 3. Dispersion relation in RVE of semi-infinite random unidirectional fiber-reinforced composites

In the two-dimensional case, when the inner thermal source is omitted, the heat conduction equation in materials is expressed as:

$$\lambda(r)\nabla^2 T + \nabla\lambda(r)\cdot\nabla T = \rho(r)c(r)\frac{\partial T(r,t)}{\partial t}, \tag{1}$$

where $\nabla$ is the nabla operator, $\nabla^2 = \partial_2/\partial x^2 + \partial^2/\partial y^2$ is the two-dimensional Laplace operator, $T(r,t)$ is the temperature in materials, and $\lambda(r)$, $c(r)$ and $\rho(r)$ are the thermal conductivity, specific heat capacity and density of materials, respectively.

The non-steady and periodical solution of the problem is investigated. Let $T = T_0 + \mathrm{Re}[\vartheta(r)\exp(-\mathrm{i}\omega t)]$, Eq. (1) can be changed into the following equation:

$$\lambda(r)\nabla^2\vartheta(r) + \nabla\lambda(r)\nabla\vartheta(r) + \mathrm{i}\omega\rho(r)c(r)\vartheta(r) = 0, \tag{2}$$

where $T_0$ is the mean temperature in materials, $\vartheta(r)$ is the amplitude of temperature, and $\omega$ is the circular frequency of thermal waves.

Suppose that $\lambda(r)$, $c(r)$, and $\rho(r)$ may be presented as the following sums:

$$\lambda(r) = \lambda_0 + \lambda\bar{s}(r), \quad \lambda_1 = \lambda - \lambda_0, \qquad c(r) = c_0 + \bar{s}(r), \quad c_1 = c - c_0,$$
$$\rho(r) = \rho_0 + \rho\bar{s}(r), \quad \rho_1 = \rho - \rho_0, \tag{3}$$

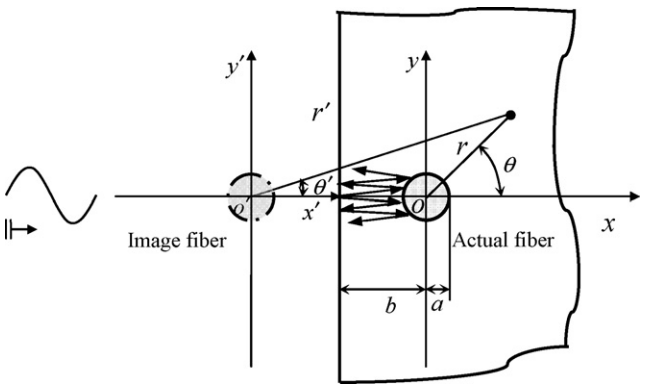


**Fig. 2.** Schematic of the wave incidence and image method in the effective medium with one-fiber.

where $\bar{s}(r)$ is the characteristic function of the region $\bar{s}$ occupied by the fibers ($\bar{s}(r) = 1$, if $r \in \bar{s}$, $\bar{s}(r) = 0$, if $r \notin \bar{s}$).

From Eqs. (2) and (3), the governing equation of temperature in the RVE can be obtained:

$$\lambda_0 \nabla^2 \vartheta(r) + \mathrm{i}\rho_0 c_0 \omega \vartheta(r) = -\nabla \lambda_1 \bar{t}(r)\bar{s}(r) - \mathrm{i}\omega\rho_1 c_1 \vartheta(r)\bar{s}(r), \tag{4}$$

where $\bar{t}(r) = \nabla\vartheta(r)$.

Applying the operator $(\lambda_0 \nabla^2 + \mathrm{i}\rho_0 c_0 \omega)^{-1}$ to both sides of Eq. (4), we obtain the integral equation for the temperature field $\vartheta(r)$ in the form:

$$\vartheta(r) = \vartheta_0(r) + \int_s [\nabla G(r-r')\lambda_1 \bar{t}(r') + \mathrm{i}\omega G(r-r')\rho_1 c_1 \vartheta(r')]s(r')\ \mathrm{d}r', \tag{5}$$

where $\vartheta_0(r)$ is the temperature field that would have existed in the medium without fibers ($\lambda = 0$, $c = 0$, $\rho = 0$), and $s$ is the whole area of the RVE. $G(r)$ is the Green function of the operator $\lambda_0 \nabla^2 + \mathrm{i}\rho_0 c_0 \omega$. Applying the image method shown in Fig. 2, it is expressed as:

$$G(r) = -\frac{i}{4\lambda_0}[H_0^{(1)}(k_0|r|) + H_0^{(1)}(k_0|r'|)], \tag{6}$$

where $|r'| = (r^2 + 4b^2 + 4br\ \cos\theta)^{1/2}$ with $b$ being the distance between the center of RVE and the semi-infinite edge, $H_0^{(1)}(\cdot)$ is the zero order Hankel function of the first kind, $k_0$ is the complex wave number of thermal waves, and $k_0 = (1+\mathrm{i})k$ with $k = \sqrt{\rho_0 c_0 \omega / 2\lambda_0}$.

According to the hypotheses of EMM [17], the interaction of temperature field between many fibers in the RVE can be reduced to the one-fiber problem. This problem is the diffraction of a monochromatic thermal wave on an isolated fiber embedded in the effective medium with the properties $\lambda_e$, $c_e$ and $\rho_e$. The effective thermal wave field is $\vartheta_e(r) = \bar{\vartheta}_e e^{\mathrm{i}(\mathbf{k}_e \cdot \mathbf{r} - \omega t)}$ with $\mathbf{k}_e = k_e \mathbf{n}$. Note that $k_e$ is the effective wave number.

Thus, the integral equation denoted by the effective temperature field in the one-fiber region is described as:

$$\vartheta(r) = \vartheta_e(r) + \int_{s_0} [\nabla G_e(r-r')\lambda_{e1}\bar{t}(r') + \mathrm{i}\omega G_e(r-r')\rho_{e1}\vartheta(r')]\ \mathrm{d}r'. \tag{7}$$

Here $s_0$ is the area of the fiber cross-section, $G_e(r)$is the Green function of effective medium, and $\lambda_{e1} = \lambda - \lambda_e$, $c_{e1} = c - c_e$, $\rho_{e1} = \rho - \rho_e$.

Let the general solution of Eq. (5) be known, and the temperature field $\vartheta(r)$ inside the fiber with the center at point $r^0 = 0$ be presented in the form:

$$\vartheta(r) = (\Lambda\vartheta_e)(r) = \Lambda[\bar{\vartheta}_e e^{\mathrm{i}\mathbf{k}_e \cdot \mathbf{r}}], \tag{8}$$

where $\Lambda$ is a linear operator that depends on the non-steady properties of the effective temperature fields and fiber.

If the fiber occupies area $S_0$ with the center at a point $r^0 \neq 0$, one can present the field $\vartheta(r)$ inside such an inclusion in the following form ($r \in s_0$):

$$\begin{aligned}\vartheta(r) &= \Lambda[\bar{\vartheta}_e e^{\mathrm{i}\mathbf{k}_e \cdot (\mathbf{r}-\mathbf{r}^0)} e^{\mathrm{i}\mathbf{k}_e \cdot \mathbf{r}^0}] \\ &= \Lambda[e^{\mathrm{i}\mathbf{k}_e \cdot (\mathbf{r}-\mathbf{r}^0)}]\bar{\vartheta}_e e^{\mathrm{i}\mathbf{k}_e \cdot \mathbf{r}^0} = \Lambda[e^{\mathrm{i}\mathbf{k}_e \cdot (\mathbf{r}-\mathbf{r}^0)}] e^{\mathrm{i}\mathbf{k}_e \cdot (\mathbf{r}-\mathbf{r}^0)} \bar{\vartheta}_e e^{\mathrm{i}\mathbf{k}_e \cdot \mathbf{r}} \\ &= \Lambda^{\vartheta}(r - r^0)\vartheta_e(r), \quad \Lambda^{\vartheta}(z) = \Lambda[e^{\mathrm{i}\mathbf{k}_e \cdot z}] e^{-\mathrm{i}\mathbf{k}_e \cdot z}.\end{aligned} \tag{9}$$

Similarly, from $\bar{t}(r) = \nabla\vartheta(r)$, the following can be obtained:

$$\begin{aligned}&\bar{t}(r) = \nabla\Lambda[\bar{\vartheta}_e e^{\mathrm{i}\mathbf{k}_e \cdot (\mathbf{r}-\mathbf{r}^0)} e^{\mathrm{i}\mathbf{k}_e \cdot \mathbf{r}^0}] = \Lambda^{\tau}(r - r^0)\vartheta_e(r), \\ &\Lambda^t(z) = \nabla\Lambda[e^{\mathrm{i}\mathbf{k}_e \cdot z}] e^{-\mathrm{i}\mathbf{k}_e \cdot z},\end{aligned} \tag{10}$$

note that $\Lambda^{\vartheta}(z)$ and $\Lambda^t(z)$ do not depend on the position $r = 0$ of the center of the fiber. They can be constructed from the solution of the one-fiber problem for the fiber centered at the point $r = 0$.

Let us introduce random functions $\chi^{\vartheta}(r)$ and $\chi^t(r)$ in the 2D-space. These functions coincide with $\Lambda^{\vartheta}(r - r^t)$ and $\Lambda^t(r - r^i)$ if $r$ is inside the fiber centered at point $r^i$ ($r = 1, 2, 3, \ldots$), and they are equal to zero in the matrix. Substitution of Eqs. (9) and (10) into Eq. (5) yields the following:

$$\begin{aligned}\vartheta(r) = \vartheta_0(r) + \int_{s_0} &[\nabla G(r-r')\lambda_1 \chi^t(r')\vartheta_e(r') \\ &+ \mathrm{i}\omega G(r-r')\rho_1 c_1 \chi^{\vartheta}(r')\vartheta_e(r')]S(r')\ \mathrm{d}r'.\end{aligned} \tag{11}$$

In order to find the mean wave field, let us average both sides of Eq. (11) over ensemble realization of the random set of fibers, and take into account the condition of $\vartheta_e(r) = \langle\vartheta(r)\rangle$, the following can be obtained:

$$\begin{aligned}\langle\vartheta(r)\rangle = \vartheta_0(r) + V_f \int &[\nabla G(r-r')\lambda_1 \Lambda^c \\ &+ \mathrm{i}\omega G(r-r')\rho_1 c_1 \Lambda_\rho]\langle\vartheta(r')\rangle\ \mathrm{d}r',\end{aligned} \tag{12}$$

$$\Lambda_\rho(k_e) = \lim_{\Omega\to\infty} \frac{1}{V_f \Omega} \int_\Omega \chi^{\vartheta}(r)\mathrm{d}r = \frac{1}{\langle s\rangle} \left\langle \int_s \Lambda^{\vartheta}(r)\ \mathrm{d}r \right\rangle, \tag{13}$$

$$\Lambda^c(k_e) = \lim_{\Omega\to\infty} \frac{1}{V_f \Omega} \int_\Omega \chi^t(r)\mathrm{d}r = \frac{1}{\langle s\rangle} \left\langle \int_s \Lambda^t(r)\ \mathrm{d}r \right\rangle, \tag{14}$$

where $\Lambda_\rho$ and $\Lambda^c$ are constant scalar and vector, respectively, $\Omega$ is the two-dimensional plane $(x,y)$ in the RVE, and $s$ is the area occupied by the typical fiber.

Let us apply the Fourier transform to Eq. (12) and multiply the result with $L_0(k) = \lambda_0 k^2 - \mathrm{i}\rho_0 c_0 \omega$. Taking into account the equations:

$$L_0(\boldsymbol{k})G(\boldsymbol{k}) = 1, \qquad L_0(\boldsymbol{k})\vartheta_0(\boldsymbol{k}) = 0, \tag{15}$$

the following can be obtained:

$$\begin{aligned}&L_e(\boldsymbol{k})\langle\vartheta(\boldsymbol{k})\rangle = 0, \quad L_e(\boldsymbol{k}) = L_0(\boldsymbol{k}) + V_f\lambda_1 \mathrm{i}k_i \Lambda^c(\boldsymbol{k}_e) - V_f\rho_1 \mathrm{i}\omega\Lambda_\rho(\boldsymbol{k}_e) \\ &-V_f c_1 \mathrm{i}\omega\Lambda_\rho(\boldsymbol{k}_e).\end{aligned} \tag{16}$$

Because the vector $\Lambda^c$ in Eq. (16) is a function of the vector $\mathbf{k}_e$ only, $\Lambda^c$ may be written as:

$$\Lambda^c(\boldsymbol{k}_e) = -\mathrm{i}k_e H_C(k_e), \quad k_e = |\boldsymbol{k}_e|, \tag{17}$$

where $H_C(k_e)$ is a scalar function. If the mean temperature field $\langle\vartheta(r)\rangle$ is a plane thermal wave ($\langle\vartheta(\boldsymbol{r})\rangle = \bar{\vartheta}_e e^{\mathrm{i}\mathbf{k}_e \cdot \mathbf{r}}$), its Fourier

transform is $\langle\vartheta(\boldsymbol{k})\rangle = (2\pi)^{-1}\bar{\vartheta}_e\delta(\boldsymbol{k}-\boldsymbol{k}_e)$, Eq. (16) takes the form $L_e(\mathbf{k})\delta(\mathbf{k}-\mathbf{k}_e)=0$, namely:

$$L_e(\boldsymbol{k}_e) = L_0(\boldsymbol{k}_e) + V_f\lambda_1(k_e)^2 H_C(k_e) - V_f\rho_1 i\omega\Lambda_\rho(k_e) - V_f c_1 i\omega\Lambda_\rho(k_e) = 0. \quad (18)$$

This equation may be simplified as:

$$\lambda_e(k_e)k_e^2 - i\omega[\rho_e(k_e)+c_e(k_e)] = 0, \quad \lambda_e(k_e) = \lambda_0 + V_f\lambda_1 H_C(k_e),$$
$$\rho_e(k_e) = \rho_0 + V_f\rho_1\Lambda_\rho(k_e), \quad c_e(k_e) = c_0 + V_f c_1\Lambda_\rho(k_e). \quad (19)$$

Note that Eq. (19) is the dispersion relation for the effective wave number $k_e$ of the mean thermal wave field in the RVE.

## 4. The one-fiber problem and image method

By using effective medium method, the multiple scattering of thermal waves between the random fibers in the matrix is reduced to the one-fiber problem in the effective wave field. To solve the multiple scattering of thermal waves around the fiber resulting from the semi-infinite surface, the image method is used to satisfy the adiabatic boundary condition at the semi-infinite surface, as shown in Fig. 2. The radius of the cylindrical fiber is $a$. The distance between the semi-infinite edge and the center of the fiber is $b$.

Let the effective thermal wave field be incident in the positive $x$ direction. The incident waves can be expressed as:

$$\vartheta_{1*}^{(i)} = \vartheta_* e^{i(\mathbf{k}_*\cdot\mathbf{r}-\omega t)} = \vartheta_*\sum_{n=-\infty}^{\infty} i^n J_n(k_* r)e^{in\theta}\ \exp(-i\omega t), \quad (20)$$

where $\vartheta_*$ is the temperature amplitude of the effective thermal wave field, and $J_n(-)$ is the $n$th Bessel function. Note that the subscript 1 denotes the wave field around the actual fiber, and the superscript $(i)$ denotes the effective incident waves.The reflected thermal wave at the edge of the semi-infinite composite structure is described by the virtual image fiber. For the image fiber, the incident waves propagate in the negative $x'$ direction, and can be expressed as:

$$\vartheta_{2*}^{(i)} = \vartheta_* e^{i(-\mathbf{k}_*\cdot\mathbf{r}-\omega t)} = \vartheta_*\sum_{n=-\infty}^{\infty} i^{-n} J_n(k_* r')e^{in\theta'}\ \exp(-i\omega t), \quad (21)$$

note that the subscript 2 denotes the effective incident waves around the image fiber.

Considering the multiple scattering of effective temperature field between the actual and image fibers, the scattered fields of thermal waves produced by the actual fiber are described, in the localized coordinate system $(r,\theta)$, as:

$$\vartheta_{1*}^{(s)} = \sum_{n=-\infty}^{\infty} A_{n1}H_n^{(1)}(k_* r)e^{in\theta}\ \exp(-i\omega t), \quad (22)$$

note that the superscript $(s)$ denotes the scattered thermal waves.

In the same way, the scattered waves produced by the image fiber, in the localized coordinate system $(r',\theta)$ of the image fiber, are described as:

$$\vartheta_{2*}^{(s)} = \sum_{n=-\infty}^{\infty} A_{n2}H_n^{(1)}(k_* r')e^{in\theta'}\ \exp(-i\omega t), \quad (23)$$

note that $A_{n1}$ and $A_{n2}$ are the modal coefficients of the scattered waves for the actual and image fibers, respectively. They are determined by satisfying the continuity boundary conditions of the fibers. In this paper, they are also dependent on the boundary conditions at the semi-infinite surface.

Likewise, the refracted thermal waves inside the actual and image fibers are standing waves, which can be described as:

$$\vartheta_{1*}^{(r)} = \sum_{n=-\infty}^{\infty} A_{n3}J_n(kr)e^{in\theta}\ \exp(-i\omega t), \quad (24)$$

$$\vartheta_{2*}^{(r)} = \sum_{n=-\infty}^{\infty} A_{n4}J_n(kr')e^{in\theta'}\ \exp(-i\omega t), \quad (25)$$

where $A_{n3}$ and $A_{n4}$ are the modal coefficients of the refracted waves for the actual and image fibers, respectively. Note that the superscript $(r)$ denotes the refracted waves.

Substituting Eq. (24) into Eqs. (12), (13) and (16), the following can be obtained:

$$\Lambda_\rho = \sum_{n=-\infty}^{\infty} A_{n3}g_n, \qquad H_C = \sum_{n=-\infty}^{\infty} A_{n3}g_{1n}, \quad (26)$$

$$g_n = \frac{2i^n}{a}\cdot\frac{1}{k^2-k_*^2}[kJ_{n+1}(ka)J_n(k_*a) - k_*J_n(ka)J_{n+1}(k_*a)], \quad (27)$$

$$g_{1n} = g_n + \frac{2i^n}{ak_*}J_n(ka)J_n'(k_*a). \quad (28)$$

According to the continuous boundary conditions of the temperature and heat-flux density around the fibers, the boundary conditions for the effective thermal waves can be written as:

$$\vartheta_{1*}^{(t)}|_{r=a} = \vartheta_{1*}^{(i)}|_{r=a} + \vartheta_{1*}^{(s)}|_{r=a} + \vartheta_{2*}^{(s)}|_{r=a} = \vartheta_{1*}^{(r)}|_{r=a}, \quad (29)$$

$$q_{r1*}^{(t)}|_{r=a} = q_{r1*}^{(i)}|_{r=a} + q_{r1*}^{(s)}|_{r=a} + q_{r'2*}^{(s)}|_{r=a} = q_{r1*}^{(r)}|_{r=a}, \quad (30)$$

$$\vartheta_{2*}^{(t)}|_{r'=a} = \vartheta_{2*}^{(i)}|_{r'=a} + \vartheta_{2*}^{(s)}|_{r'=a} + \vartheta_{1*}^{(s)}|_{r'=a} = \vartheta_{2*}^{(r)}|_{r'=a}, \quad (31)$$

$$q_{r'2*}^{(t)}|_{r'=a} = q_{r'2*}^{(i)}|_{r'=a} + q_{r'2*}^{(s)}|_{r'=a} + q_{r1*}^{(s)}|_{r'=a} = q_{r'2*}^{(r)}|_{r'=a}, \quad (32)$$

where $\vartheta_{1*}^{(t)}$ is the total temperature field around the actual fiber, and $q_{r1*}^{(t)} = -\lambda_*(\partial\vartheta_{1*}^{(t)}/\partial r)$ is the total heat-flux density around the actual fiber.

To make the computation tractable, the expressions of thermal waves in the localized coordinate system $(r',\theta)$ should be translated into the coordinate system $(r,\theta)$. According to the addition theorem of Graf [21], the following relations can be derived:

$$H_n^{(1)}(kr')e^{in\theta'} = \sum_{m=-\infty}^{\infty}(-1)^{m-n}H_{m-n}^{(1)}(2kb)J_m(kr)e^{im\theta}, \quad (33)$$

similarly:

$$H_n^{(1)}(kr)e^{in\theta} = \sum_{m=-\infty}^{\infty}H_{m-n}^{(1)}(2kb)J_m(kr')e^{im\theta'}. \quad (34)$$

The expressions of the temperature and heat-flux density are substituted into Eqs. (29)–(32). Multiplying $e^{-is\theta}$ on both sides of Eqs. (29)–(32), and then integrating over $\theta\in[-\pi,\pi]$, a set of algebraic equation system is obtained. After arrangement, the equations can be simplified as:

$$[E]\{A\} = \{f\}, \quad (35)$$

where $E$ is a coefficient matrix of $4\times4$, and $f$ is a vector of 4 ranks, whose elements are shown in Appendix A. After solving the linear equation system (35), the modal coefficients $A_{s1}$, $A_{s2}$, $A_{s3}$ and $A_{s4}$ ($s=0,\pm1,\pm2,\ldots$) can be obtained.

## 5. Determination of non-steady effective thermal properties

According to the dispersion relation in Eq. (19), we construct the numerical solutions of the effective thermal properties. Based

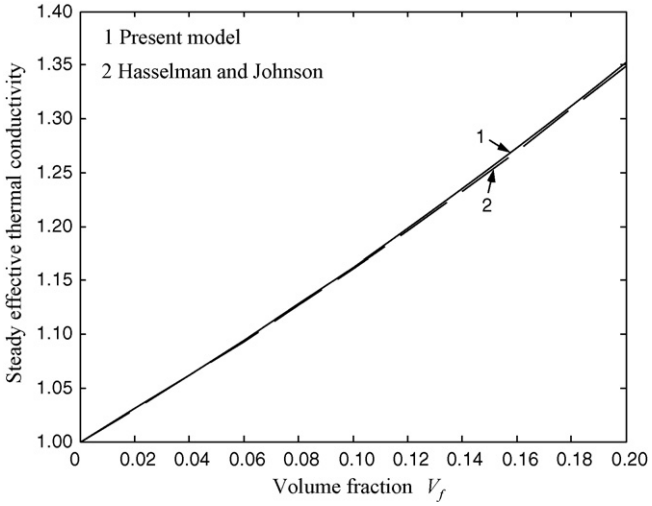


**Fig. 3.** Comparison of the steady effective thermal conductivity with Hasselman and Johnson (Ref. [11]) ($\lambda^* = 5.0$, $c^* = 2.0$, $\rho^* = 2.0$, $k^* = 0$).

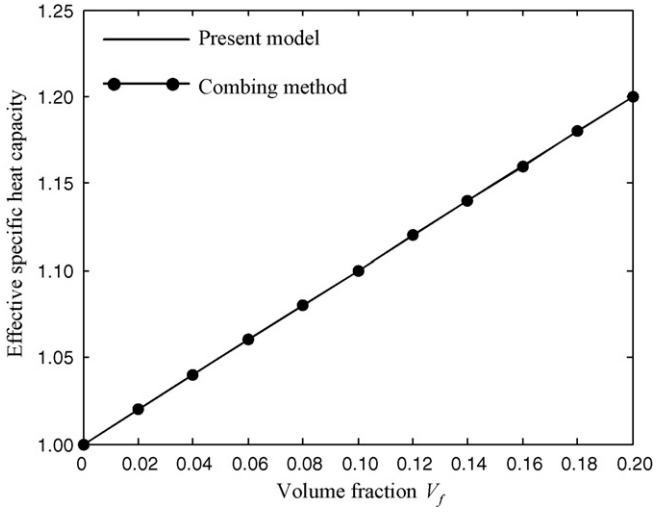


**Fig. 4.** Comparison of the effective specific heat capacity with the combing method under steady state ($\lambda^* = 5.0$, $c^* = 2.0$, $\rho^* = 2.0$, $k^* = 0$).

on Eq. (19), the numerical solutions are obtained by the iterative procedure, i.e.

$$\lambda_e^n = \lambda_e^{n-1} + \varepsilon[\lambda_e^{n-1} - \lambda_0(1 + V_f\bar{\lambda}H_C(k_e^{n-1}, \lambda_e^{n-1}))], \tag{36}$$

$$\rho_e^n = \rho_e^{n-1} + \varepsilon[\rho_e^{n-1} - \rho_0(1 + V_f\bar{\rho}_1\Lambda_\rho(k_e^{n-1}, \rho_e^{n-1}))], \tag{37}$$

$$c_e^n = c_e^{n-1} + \varepsilon[c_e^{n-1} - c_0(1 + V_f\bar{c}_1\Lambda_\rho(k_e^{n-1}, c_e^{n-1}))], \tag{38}$$

$$k_e^n = (1+i)\left(\frac{\rho_e^n c_e^n \omega}{2\lambda_e^n}\right)^{1/2}, \quad \bar{\lambda} = \frac{\lambda_1}{\lambda_0}, \quad \bar{\rho} = \frac{\rho_1}{\rho_0}, \quad \bar{c} = \frac{c_1}{c_0}, \tag{39}$$

where $k_e^n$, $\lambda_e^n$, $c_e^n$ and $\rho_e^n$ are the effective parameters for the $n$th iteration, and functions $H_C(k_e,\lambda_e)$, $\Lambda_\rho(k_e,\rho_e)$ and $\Lambda_\rho(k_e,c_e)$ are defined in Eqs. (26)–(28). Parameter $\varepsilon(|\varepsilon| < 1)$ is to be chosen for conversion of the iterative process. As an initial (zero) approximation, the static solutions $k_e^{(0)} = (1+2i)\sqrt{[(\rho_0+\rho_1)V_f][c_0+c_1V_f]\omega/\lambda_s}$ and $\lambda_e^{(0)} = \lambda_s$ are applied. $\lambda_s$ is the static thermal conductivity, and is proposed as [11]:

$$\lambda_s = \lambda_0\left[1 + \frac{\alpha V_f[1 + V_f\beta^2/4] + [1 - V_f]}{\alpha V_f(\lambda_0/\lambda)[1 + V_f\beta^2/4] + [1 - V_f]}\right], \tag{40}$$

where $\alpha = 3\lambda/(\lambda + 2\lambda_0)$, $\beta = (\lambda - \lambda_0)/(\lambda + 2\lambda_0)$.

## 6. Numerical examples

To find the effect of the semi-infinite surface, the volume fraction of fibers, the wave frequency of thermal waves, and the thermal property contrast ratio of the two phases on the non-steady effective thermal properties of the composite, the numerical examples are given. In the following analysis, it is convenient to make the variables dimensionless. To accomplish this step, we may introduce a representative length scale $a$, where $a$ is the radius of the reinforcing fibers. The following dimensionless variables and quantities have been chosen for computation: $k^* = k_0 a = 0.1$–$5.0$, $X^* = X/a = 1.0$–$10.0$, $\lambda^* = \lambda/\lambda_0 = 0.1$–$10.0$, $c^* = c/c_0 = 0.1$–$5.0$, and $\rho^* = \rho/\rho_0 = 0.1$–$5.0$. The dimensionless effective thermal conductivity is $\lambda_e^* = \lambda_e/\lambda_0$, The dimensionless specific heat capacity is $c_e^* = c_e/c_0$.

To validate this thermodynamic model, the steady effective thermal conductivity of two-phase composites is given in Fig. 3. As $k^* \to 0$, the non-steady effective thermal conductivity tends to the steady solutions. In Fig. 3, the results obtained from the present model, and Hasselman and Johnson [11] are plotted. Close agreement is seen to exist between the two models.

When $k^* = 0$, comparison of the effective specific heat capacity with the combing method is also illustrated in Fig. 4. It can be seen that the agreement between the two methods is very good.

In Figs. 5 and 6, we plot respectively the non-steady effective thermal conductivity and specific heat capacity of the semi-infinite composite material under different dimensionless wave number as a function of $X^*$ with parameters: $\lambda^* = 10.0$, $c^* = \rho^* = 2.0$ and $V_f = 0.1$. It can be seen that the non-steady effective thermal conductivity and specific heat capacity decrease with the increase of $X^*$. The maximum values of non-steady effective thermal conductivity and specific heat capacity occur at the semi-infinite surface. The phenomenon results from the multiple scattering of thermal waves between the semi-infinite surface and the fibers. Near the semi-infinite surface, the multiple scattering of thermal waves is strong. With the increase of the value of $X^*$, the diffusion of thermal waves from the randomly distributed fibers becomes greater and greater. So, the non-steady effective thermal conductivity decreases with the increase of $X^*$. Near the semi-infinite surface, the non-steady effective thermal properties increase with the incident frequency of thermal waves. With the increase of the value of $X^*$, the effect of the incident frequency of thermal waves becomes weak. It is also clear that the greater the incident frequency of thermal waves, the

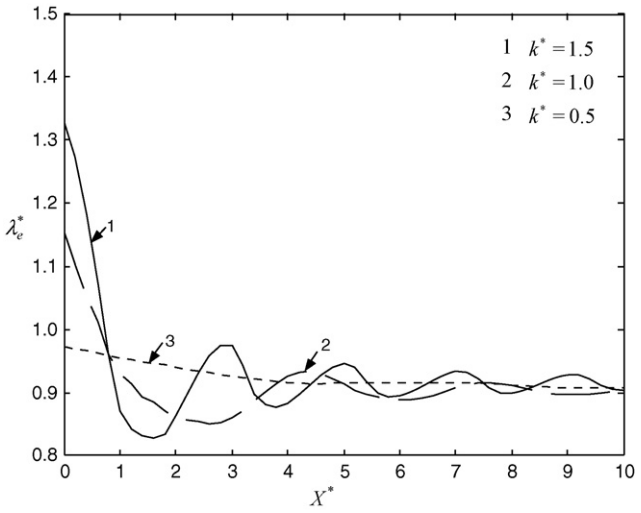


**Fig. 5.** Effect of wave frequency on non-steady effective thermal conductivity ($\lambda^* = 10.0$, $c^* = 2.0$, $\rho^* = 2.0$, $k^* = 0.1$).

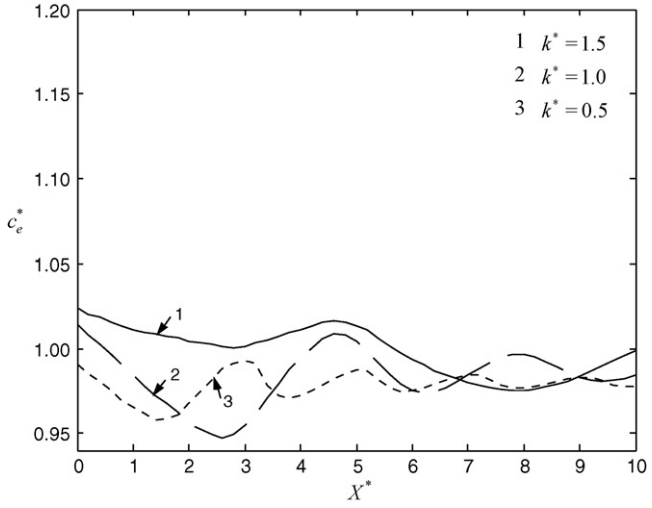


**Fig. 6.** Effect of wave frequency on effective specific heat capacity ($\lambda^*=10.0$, $c^*=2.0$, $\rho^*=2.0$, $V_f=0.1$).

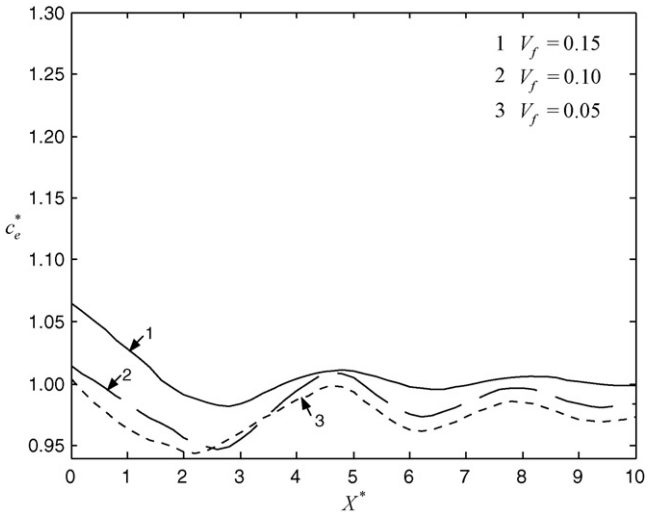


**Fig. 8.** Effect of volume fraction of fibers on effective specific heat capacity ($\lambda^*=10.0$, $c^*=2.0$, $\rho^*=2.0$, $k^*=1.0$).

greater the effect of the semi-infinite boundary on the non-steady effective thermal properties.

Comparing the results in Figs. 5 and 6, it can be seen that the effect of thermal wave frequency on the non-steady effective thermal conductivity is greater than that on the non-steady effective specific heat capacity.

In Figs. 7 and 8, we plot respectively the non-steady effective thermal conductivity and specific heat capacity of the semi-infinite composites under different volume fraction of fibers as a function of $X^*$ with parameters: $\lambda^*=10.0$, $c^*=\rho^*=2.0$, and $k^*=1.0$. It can be seen that the non-steady effective thermal properties near the semi-infinite surface increase with the increase of the volume fraction of fibers. However, when the value of $X^*$ is greater, the non-steady effective thermal properties decreases with the increase of the volume fraction of fibers, and the variations of them with the volume fraction of fibers are little. This phenomenon results from the diffraction and attenuation of thermal waves.

Comparing the results in Figs. 7 and 8, it can be seen that the effect of volume fraction of fibers on the non-steady effective thermal conductivity is greater than that on the non-steady effective specific heat capacity.

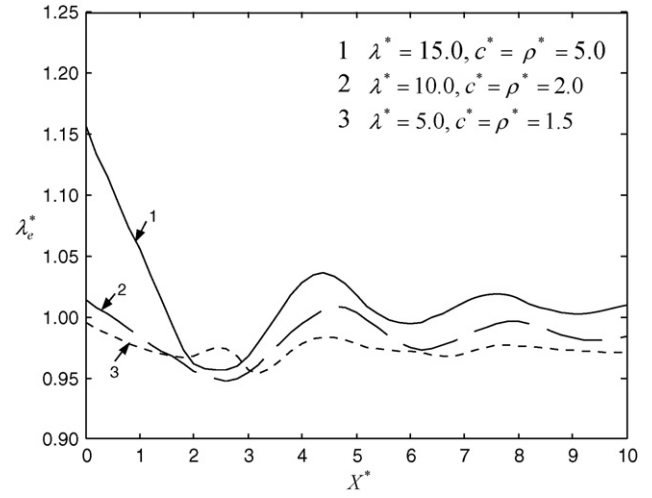


**Fig. 9.** Effect of properties contrast ratio of the two phases on non-steady effective thermal conductivity ($k^*=1.0$, $V_f=0.10$).

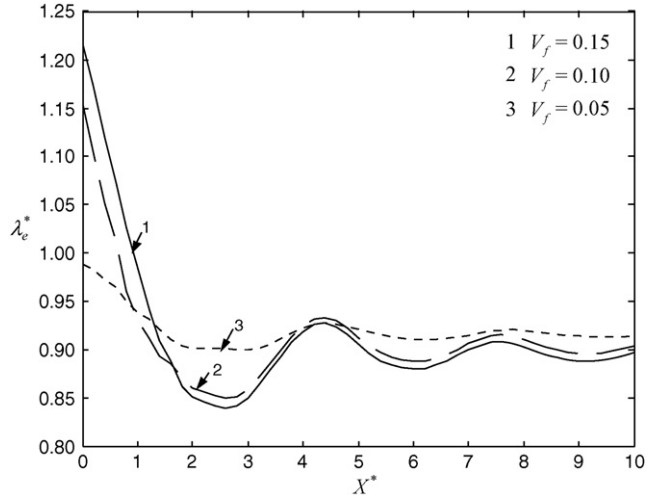


**Fig. 7.** Effect of volume fraction of fibers on non-steady effective thermal conductivity ($\lambda^*=10.0$, $c^*=2.0$, $\rho^*=2.0$, $k^*=1.0$).

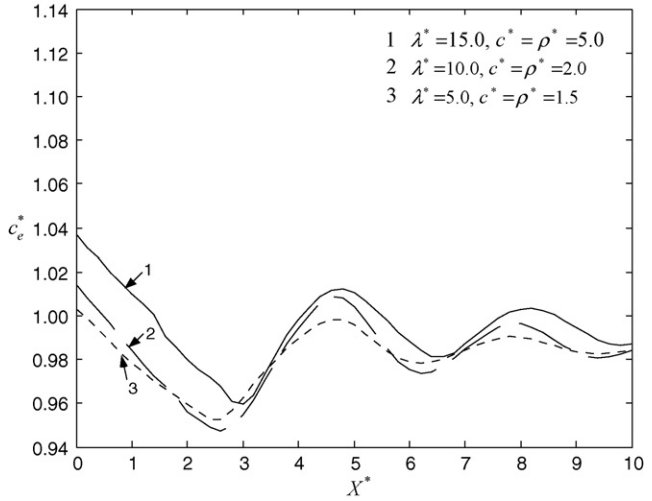


**Fig. 10.** Effect of properties contrast ratio of the two phases on effective specific heat capacity ($k^*=1.0$, $V_f=0.10$).

To illustrate the effect of properties contrast ratio of the two phases on the non-steady effective thermal properties of the semi-infinite composite structure, Figs. 9 and 10 are plotted. It can be seen that the non-steady effective thermal properties in the composite structure increase with the increase of the properties contrast ratio of the two phases. Near the semi-infinite surface, the variations of non-steady effective thermal properties with the properties contrast ratio of the two phases are greater. Comparing the results in Figs. 9 and 10, it can be seen that the effect of properties contrast ratio of the two phases on the non-steady effective thermal conductivity is greater than that on the non-steady effective specific heat capacity.

## 7. Conclusion

Photothermal techniques are presented to analyze the non-steady effective thermal properties of semi-infinite random unidirectional fiber-reinforced composites. By using effective medium method, the problem of random media is simplified to the one-fiber problem, and the dispersion relation in the semi-infinite random composites is obtained. The one-fiber problem is solved by employing the wave function expansion method and the image method. The numerical examples of the non-steady effective properties of the semi-infinite composite structure are graphically presented. The satisfactory agreement with the static solution has been observed.

It has been found that the non-steady effective thermal conductivity and specific heat capacity decrease with the increase of $X^*$. The maximum values of non-steady effective thermal conductivity and specific heat capacity occur at the semi-infinite surface. The greater the incident frequency of thermal waves, the greater the effect of the semi-infinite boundary on the non-steady effective thermal properties. With the increase of the value of $X^*$, the effect of the incident frequency of thermal waves becomes weak. The non-steady effective thermal properties near the semi-infinite surface increase with the increase of the volume fraction of fibers and the properties contrast ratio of the two phases. Near the semi-infinite surface, the variations of non-steady effective thermal properties with the volume fraction of fibers and the properties contrast ratio of the two phases are greater. Through comparison, it is also found that the effects of wave frequency, the volume fraction of fibers and the properties contrast ratio of the two phases on the non-steady effective thermal conductivity are greater than that on the non-steady effective specific heat capacity.

## Appendix A.

The elements of coefficient matrix $E$ and vector $f$ are given by:

$$E^{11} = H_s^{(1)}(k_*a), \tag{A1}$$

$$E^{12} = \sum_{n=-\infty}^{\infty} (-1)^{s-n} H_{s-n}^{(1)}(2kb) J_s(k_*a), \tag{A2}$$

$$E^{13} = J_s(ka), \tag{A3}$$

$$E^{14} = 0, \tag{A4}$$

$$f^1 = -\mathrm{i}^s J_s(k_*a), \tag{A5}$$

$$E^{21} = \lambda_* \frac{k_*}{2} [H_{s-1}^{(1)}(k_*a) - H_{s+1}^{(1)}(k_*a)], \tag{A6}$$

$$E^{22} = \sum_{n=-\infty}^{\infty} (-1)^{s-n} H_{s-n}^{(1)}(2kb) \lambda_* \frac{k_*}{2} [J_{s-1}(k_*a) - J_{s+1}(k_*a)], \tag{A7}$$

$$E^{23} = \frac{\lambda_0 k}{2} [J_{s-1}(ka) - J_{s+1}(ka)], \tag{A8}$$

$$E^{24} = 0, \tag{A9}$$

$$f^2 = -\mathrm{i}^s \frac{\lambda_* k_*}{2} [J_{s-1}(k_*a) - J_{s+1}(k_*a)], \tag{A10}$$

$$E^{31} = \sum_{n=-\infty}^{\infty} H_{s-n}^{(1)}(2kb) J_s(k_*a), \tag{A11}$$

$$E^{32} = H_s^{(1)}(k_*a), \tag{A12}$$

$$E^{33} = 0, \tag{A13}$$

$$E^{34} = J_s(ka), \tag{A14}$$

$$f^3 = -\mathrm{i}^{-s} J_s(k_*a), \tag{A15}$$

$$E^{41} = \sum_{n=-\infty}^{\infty} H_{s-n}^{(1)}(2kb) \frac{\lambda_* k_*}{2} [J_{s-1}(k_*a) - J_{s+1}(k_*a)], \tag{A16}$$

$$E^{42} = \frac{\lambda_* k_*}{2} [H_{s-1}^{(1)}(k_*a) - H_{s+1}^{(1)}(k_*a)], \tag{A17}$$

$$E^{43} = 0, \tag{A18}$$

$$E^{44} = \frac{\lambda_0 k}{2} [J_{s-1}(ka) - J_{s+1}(ka)], \tag{A19}$$

$$f^4 = -\mathrm{i}^{-s} \frac{\lambda_* k_*}{2} [J_{s-1}(k_*a) - J_{s+1}(k_*a)]. \tag{A20}$$

## References


[1] Y. Xu, K. Yagi, Comp. Mater. Sci. 30 (2004) 242–250.
[2] A. Salazar, J.M. Terrón, A. Sánchez-Lavega, R. Celorrio, Appl. Phys. Lett. 80 (2002) 1903–1905.
[3] M. Monde, Y. Mitsutake, Int. J. Heat Mass Transfer 44 (2001) 3169–3177.
[4] C. Hu, X.-Q. Fang, Thermochim. Acta 464 (2007) 16–23.
[5] X.-Q. Fang, C. Hu, Comp. Mater. Sci. 42 (2008) 194–202.
[6] J.C. Maxwell, A Treatise on Electricity and Magnetism, vol. 1, third ed., Dover, New York, 1954.
[7] R.P.A. Rocha, M.E. Cruz, Numer. Heat Tr. A: Appl. 39 (2001) 179–203.
[8] M. Christon, P.J. Burns, R.A. Sommerfeld, Numer. Heat Tr. A: Appl. 25 (1994) 259–278.
[9] P.K. Samantray, P. Karthikeyan, K.S. Reddy, Int. J. Heat Mass Transfer 49 (2006) 4209–4219.
[10] A. Bagchi, S. Nomura, Compos. Sci. Technol. 66 (2006) 1703–1712.
[11] D.H.P. Hasselman, L.F. Johnson, J. Compos. Mater. 21 (1987) 508–515.
[12] Z. Hashin, J. Compos. Mater. 2 (1968) 284–300.
[13] J.M. Terrón, A. Sánchez-Lavega, A. Salazar, J. Appl. Phys. 89 (2001) 5659–5702.
[14] J.M. Terrón, A. Sánchez-Lavega, A. Salazar, J. Appl. Phys. 87 (2000) 2600–2607.
[15] F. Garrido, A. Salazar, J. Appl. Phys. 95 (2004) 140–149.
[16] X.Q. Fang, C. Hu, W.H. Huang, ASME J. Appl. Mech. 74 (2007) 382–387.
[17] X.Q. Fang, C. Hu, S.Y. Du, Theor. Appl. Fract. Mech. 46 (2006) 166–174.
[18] S.K. Kanaun, V.M. Levin, Int. J. Solids Struct. 40 (2003) 4859–4878.
[19] S. Biwa, S. Yamamoto, F. Kobayashi, N. Ohno, Int. J. Solids Struct. 41 (2004) 435–457.
[20] A. Chan, X.L. Liu, W.K. Chiu, Comp. Struct. 75 (2006) 185–191.
[21] J.A. Stratton, Electromagnetic Theory, McGraw-Hill, New York, 1941.